PCCP

Kinetics of associative detachment of O- + N2 and dissociative attachment of e- + N2O up to 1300 K: Chemistry relevant to modeling of transient luminous events

Journal:	*Physical Chemistry Chemical Physics*
Manuscript ID	CP-ART-08-2023-003856.R1
Article Type:	Paper
Date Submitted by the Author:	06-Oct-2023
Complete List of Authors:	Shuman, Nicholas; Air Force Research Laboratory, Miller, Thomas; Boston College Institute for Scientific Research Ard, Shaun; Air Force Research Laboratory Viggiano, Albert; Air Force Research Laboratory, Space Vehicles Directorate

Kinetics of associative detachment of $O^- + N_2$ and dissociative attachment of $e^- + N_2O$ up to 1300 K: Chemistry relevant to modeling of transient luminous events

Nicholas S. Shuman,[1]* Thomas M. Miller,[2] Shaun G. Ard,[1] and Albert A. Viggiano[1]

[1]Air Force Research Laboratory, Space Vehicles Directorate, Kirtland AFB, New Mexico 87117, USA
[2]Boston College Institute for Scientific Research, Boston, Massachusetts 02549, USA

*Corresponding author: rvborgmailbox@us.af.mil

Abstract

The rate constants of $O^- + N_2 \rightarrow N_2O + e^-$ from 800 K to 1200 K and the reverse process $e^- + N_2O \rightarrow O^- + N_2$ from 700 K to 1300 K are measured using a flowing afterglow – Langmuir probe apparatus. The rate constants for $O^- + N_2$ are well described by $3\times10^{-12}\ e^{-0.28\ eV\ /\ kT}\ cm^3\ s^{-1}$. The rate constants for $e^- + N_2O$ are somewhat larger than previously reported and are well described by $7\times10^{-7}\ e^{-0.48\ eV\ /\ kT}\ cm^3\ s^{-1}$. The resulting equilibrium constants differ from those calculated using the fundamental thermodynamics by factors of 2-3, likely due to significantly non-thermal product distributions in one or both reactions. The potential surfaces of N_2O and N_2O^- are calculated at the CCSD(T) level. The minimum energy crossing point is identified 0.53 eV above the N_2O minimum, similar to the activation energy for the electron attachment to N_2O. A barrier between N_2O^- and $O^- + N_2$ is also identified with a transition state at a similar energy of 0.52 eV. The activation energy of $O^- + N_2$ is similar to one vibrational quantum of N_2. The calculated potential surface supports the notion that vibrational excitation will enhance reaction above the same energy in translation, and vibrational-state specific rate constants are derived from the data. The $O^- + N_2$ rate constants are much smaller than literature values measured in a drift tube apparatus, supporting the contention that those values were overestimated due to the presence of vibrationally excited N_2. The result impacts the modeling of transient luminous events in the mesosphere.

Introduction

Transient Luminous Events (TLE) are a collection of electrical phenomena that occur in the mesosphere (i.e. ~50 – 100 km altitude) above tropospheric thunderstorms.[1] Since their first identification in 1990, a large body of work (see ref. 1) has emerged to characterize the nature, cause, and effects of TLE. Notably, these discharges occur at much lower pressures than does lightning in the troposphere, and multiple groups have highlighted the resulting increased importance of associative detachment events.[2–4] Specifically, as pressure decreases, the reaction

$$O^- + N_2 \rightarrow N_2O + e^- \quad (1)$$

is assumed to become dominant over association with O_2 for the fate of O^-, reforming free electrons and affecting breakdown. Janalizadeh and Pasko[5] (J&P) point out that despite the newly identified importance of reaction 1, kinetic models rely entirely on values from a 1978 drift tube experiment by Rayment and Moruzzi (R&M).[6] J&P present a detailed analysis of the R&M experiment concluding that vibrationally excited nitrogen was present, artificially increasing the reported reaction rate constants. The recent interest in the measurement is large (R&M received 9 citations in the first 30 years after publication, but 22 further citations since 2010) and updated studies are warranted.

An upper limit on the rate constant of reaction 1 at room temperature of 10^{-12} cm^3 s^{-1} was reported by Ferguson and co-workers in their early flowing afterglow work.[7] The same group at NOAA later implemented a flow-drift tube apparatus and reiterated that upper limit over the range of kinetic energies up to 1 eV.[8] This was in contrast to a study using an ion beam apparatus reporting rather substantial cross-sections approaching low energies and implied a room temperature rate constant of ~10^{-11} cm^3 s^{-1}.[9] The later drift tube data from R&M rise to an apparent asymptote of ~10^{-12} cm^3 at the highest field strengths investigated. The result is consistent with the upper limit determined by the NOAA group, but just barely so. A second study by Moruzzi and co-workers with a distinct drift tube apparatus reported a consistent result at low field strength, approximating a room temperature rate constant of 3×10^{-13} cm^3 s^{-1}, as well as an upper limit of 3×10^{-11} cm^3 s^{-1} for reaction with $N_2(v=1)$.[10]

We are unaware of relevant studies more recent than 1982; however, there are several studies of the reverse process,[11–15] dissociative attachment to N_2O

$$N_2O + e^- \rightarrow O^- + N_2 . \quad (2)$$

It is possible that kinetic information on reaction 1 can be derived from the kinetics of reaction 2 through the fundamental thermodynamics. Moruzzi et al.[16] suggested that microscopic reversibility sets an upper limit to the room temperature rate constant for reaction 1 to yield N_2O (v=0) of 10^{-19} cm^3 s^{-1}. However, the argument is complicated because product states from both reactions 1 and 2 are undetermined and the effects of vibrational excitation unclear.

Reported rate constants for reaction 1 are scarce because the process is very inefficient and therefore difficult to measure. Whether the results of R&M are due to translational or vibrational excitation, the rate constant appears likely to increase significantly with increasing temperature. Here we report the rate constants of reaction 1 and 2 under thermal conditions at elevated temperatures up to 1300 K. This does not meet the condition suggested by J&P that only $N_2(v=0)$ be present, but rather approaches the question by having a well-determined thermal population of $N_2(\upsilon)$ varying with temperature. Because the thermodynamics of the system are very well determined, the equilibrium can be calculated and the extent to which microscopic reversibility can be used to relate the gas-phase results can

be assessed. The experiments are supported by quantum chemical calculations of the neutral and anion potential energy surfaces.

Methods

Experimental

Experiments were conducted on a high-temperature flowing afterglow – Langmuir probe (HT-FALP) apparatus that has been described previously.[17] Measurement of reactions 1 and 2 utilized different plasma sources. For reaction 1, He gas (99.999%, Matheson) metered at 12 std. L min^{-1} using a mass flow controller (MKS) and N_2O (99.99%, Matheson) metered at typically 0.1 std cm^3 min^{-1} passed through an electron-bombardment ion source containing a hot tungsten filament, yielding a weakly-ionized (~10^9 cm^{-3}) ion-electron plasma. For reaction 2, the He was passed through a microwave discharge. In both cases, Ar (99.999%, Matheson) was added downstream of the discharge at a minimum of 200 std cm^3 min^{-1} to convert He_2^+ and metastable He* into Ar^+, leaving Ar^+ along with some He^+ dominating the cation component of the plasma. The flow entered a 1.2-m long, 7-cm diameter quartz flow tube passing through a commercial oven (Mellen Co.). The electron density along the center axis was measured using a movable Langmuir probe (51-μm diameter, 8-mm long, W wire). The flow tube was heated in three independent zones such that the gas temperature from a reactant inlet halfway along the flow tube to the terminus of the flow tube was roughly constant at the desired temperature, as determined in separate experiments using a thermocouple movable along the center axis of the flow tube. The upstream zone is needed to heat the buffer gas to desired temperature prior to the reactant inlet. The temperature decreases rapidly through the final 4 cm prior to the terminus of the flow tube, as it exits the oven. To minimize this effect, heating rods were added to the downstream end of the oven. In this apparatus, we tend to use a flow tube pressure equal to T/300 Torr (T in K), such that the gas number density in the flow tube is unchanged. Some variation in the number density occurs because the Ar flow was increased with T in order to keep the ambipolar diffusion rate low, as described in Ref. [17]. In the present experiments the pressure was often lower (e.g., 2 Torr at 800 K) so that the concomitant higher flow velocity improved the O^- ion signal. The reactant inlet consisted of a 5 mm diameter quartz tube running from the upstream end of the flow tube to a circular quartz racetrack with four needle openings 63 cm prior to the terminus of the flow tube, which allows for addition of N_2 (99.9999, Matheson) or N_2O through a mass flow controller (MKS). At the end of the flow tube, the bulk of the gas flow was removed using a Roots pump while the center of the flow was sampled through a 0.2-mm aperture in a rounded nose cone into a high vacuum region. Relative ion concentrations were measured using a quadrupole mass filter and electron multiplier.

The behavior of N_2O in a discharge has been recently characterized.[18] On the timescale of μs, several anions N_2O^-, NO^-, and O^- are produced. At the helium densities here, NO^- collisionally detaches with a half-life of about 100 μs,[19] and no NO^- was observed on the ms timescales of the experiment. N_2O^- was not observed, as thermal detachment is likely at the elevated temperatures of these experiments. O^- is longer-lived under these conditions and was observed. N_2O will convert O^- to NO^-, which will then undergo detachment, requiring that minimal N_2O flow be used. In our experiment, the flow of N_2O through the electron-beam plasma source was typically 0.004 std cm^3 min^{-1} from a weak mixture of N_2O in He to achieve optimal O^- signal downstream. Adding additional N_2O was unfavorable for O^- production consistent with the reactions discussed in the previous sentence

This technique did not convert all negative charge to O^-. Besides electrons detected by the Langmuir probe, anions due to impurities were observed. Other mass peaks were observed at 26, 35, 37, 42, and 46 Da. The peaks at 26 and 42 Da were CN^- and probably CNO^- presumably from impurities in the He or Ar. The 42 Da peak could also be N_3^-, the source of which is not clear, but is a product of $N_2H^- + N_2O$ as is also OH^-, which is observed at smaller intensity.[20] A Cl^- peak at 35 and 37 Da were due to remnant chlorine-containing species from prior experiments. A small air leak with the N_2O present created NO_2^- at 46 Da. None of these are surprising since they represent a small amount of the negative charge with the bulk being electrons.

The presence of these species was used advantageously. Normally addition of a reactive gas is limited to <1% of the buffer to avoid disturbing the flow dynamics. Addition of 1% N_2 led to little decay in the O^- signal, so instead we added up to 10% (preheated) of the buffer which caused a measurable decay in the ion signals overall, but notably a steeper decrease in the O^- signal. Causes of the overall decrease in signal would be either altered diffusion, changing flow dynamics, or changes in the plasma potential. Because each impurity ion is unreactive with N_2, the relative decrease in O^- ($[O^-]/\Sigma$[impurity anions]) as a function of N_2 concentration determines the rate constant of reaction 1.

Data was taken both with and without SF_6 present in the flow tube at ~10^{10} cm^{-3}. SF_6 rapidly attaches electrons producing primarily SF_5^- at temperatures above 600 K, which decomposes to yield F^- at the higher temperatures studied here.[21–23] Without SF_6 present, electrons either remnant from the initial plasma or produced by reaction 1 can reform O^- via reaction 2 complicating determination of the rate constant. At low N_2O concentrations, this potential artifact is small.

The electron attachment measurements were made using the same apparatus with a procedure described previously.[11]

Calculations

Quantum chemical calculations were performed using the Gaussian 16 software.[24] Points on the potential energy surfaces of N_2O and of N_2O^- were calculated at CCSD(T)/aug-cc-pVTZ. Coordinates are defined as shown in Figure 1 being r_{NN}, r_{NO}, and Θ. ~4500 points were calculated over the region r_{NN} = 0.9 to 1.5 Å, r_{NO} = 0.9 – 3.0 Å, Θ = 70 – 180° (coordinates as shown in Figure 1). Calculated energies are available in the SI. Several stationary points were optimized at the same level of theory, and the energies calculated at the CCSD(T)/CBS level extrapolated to the complete basis set limit from aug-cc-pVXZ X=T, Q, 5. Stationary point geometries, energies, and frequencies are provided in the SI.

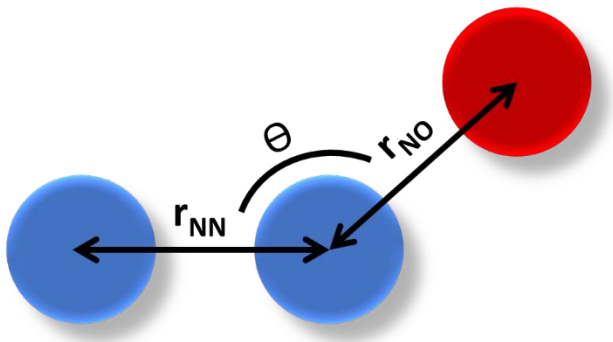

Figure 1. Coordinate scheme for potential energy diagrams below.

Results

Representative data for the determination of the rate constant of reaction 1 appears in Figure 2 at 800 and 1200 K. These are the relative abundances of the indicated species (determined from the height of the peaks in the quadrupole mass spectra, see SI) as a function of the N_2 concentration. As the N_2 concentration increases to large amounts (up to ~10% of the buffer concentration, required for sufficient extent of reaction to probe rate constant as small as $\sim 10^{-14}$ cm^3 s^{-1}), changes in the diffusion rate affect the concentrations of all ions. The decline in the raw O^- signal does not follow a single exponential decay, as it is a function of both reaction 1 and the change in diffusion rate. However, the decline in the abundance of the O^- peak relative to the impurity anion peaks does follow a single exponential decay, while the ratios of all impurity anion peaks to one another are constant as a function of N_2 concentration. We conclude that the diffusion effects are consistent across ions, all impurity anions are unreactive with N_2, and the additional decline in the O^- signal reflects the rate of reaction 1. That the impurity anions are unreactive is expected as O^- is the only ion present that has an exothermic reaction channel available. Constant flows of N_2O and SF_6 are present, resulting in concentrations of $\sim 10^{11}$ cm^{-3} and $\sim 10^{12}$ cm^{-3}, respectively. The reaction of $O^- + N_2O$ to yield $NO^- + NO$ occurs to a small, but consistent extent. NO^- is not observed because the electron is detached rapidly through collisions with the buffer gas. SF_6 efficiently scavenges electrons, such that the reaction 2 does not reform O^-. The modeled fits (Figure 2) assuming only this chemistry reproduce the data well. Derived rate constants and uncertainties for reaction 1 appear in Table I and Figure 3.

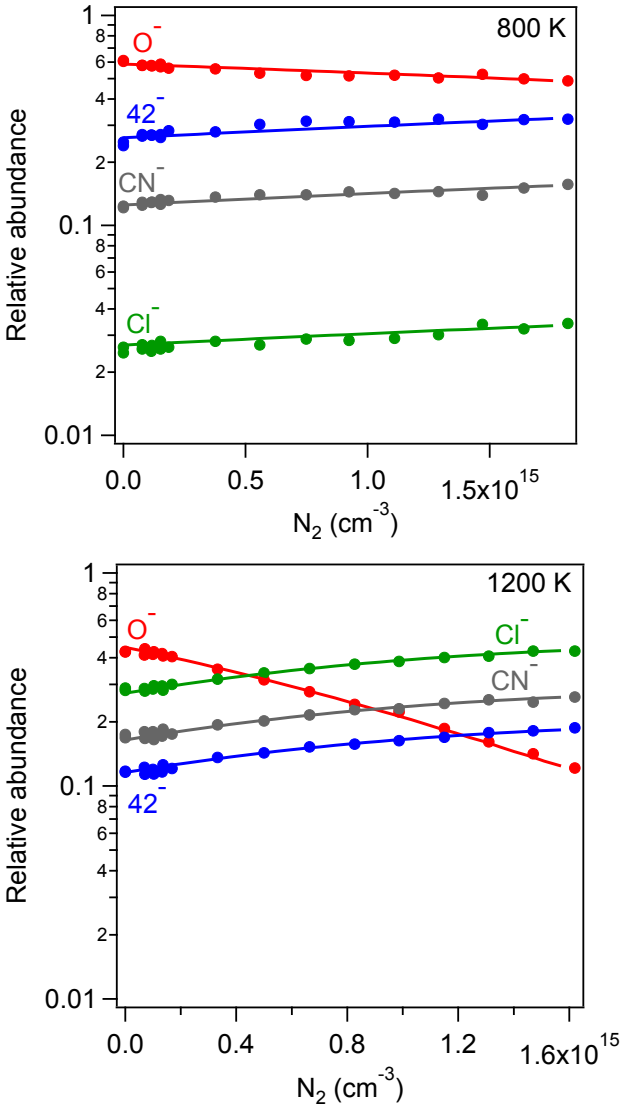

Figure 2. Representative data for measurement of reaction 1, $O^- + N_2$ at 800 K (top) and 1200 K (bottom). Measured relative abundances (solid points) of the indicated species as a function of N_2 concentration along with modeled fits (solid curves) as described in the text. Reactions times are 5.9 ms (top) and 5.3 ms (bottom).

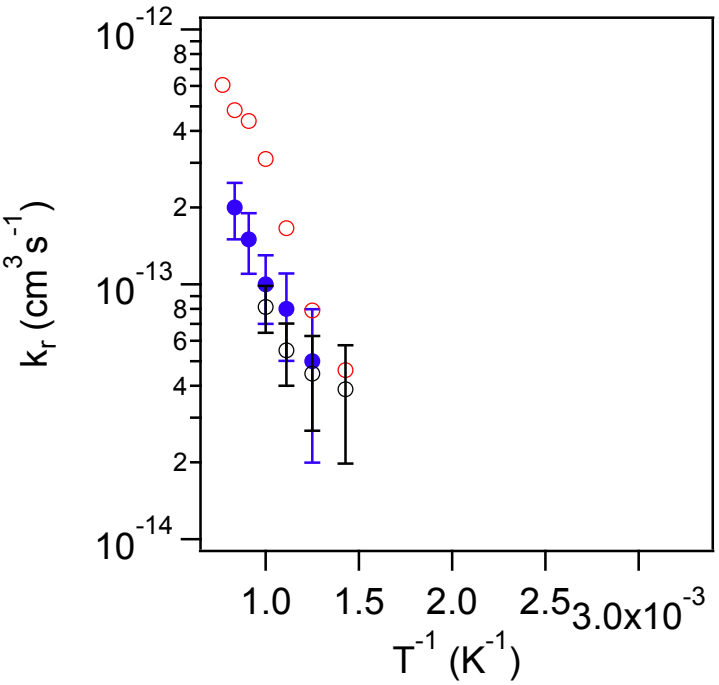

Figure 3. Measured k_{O^-+N2} as a function of inverse temperature (blue solid circles) along with values derived from equilibrium with k_{N2O+e^-} from the present data (open red circles) and previously published data (open black circles).

Table 1. Rate constants for reaction 1 $O^- + N_2$ and reaction 2 $N_2O + e^-$ at the indicated temperatures along with the derived equilibrium from both the experiment and the fundamental thermodynamics.

T (K)	k_1 (cm^3 s^{-1}) $O^- + N_2$	k_2 (cm^3 s^{-1}) $N_2O + e^-$	$K_{exp} = k_1/k_2$	K_{calc}
700	-	2.5×10^{-10}	-	1.85×10^{-4}
800	5×10^{-14}	6.0×10^{-10}	8×10^{-5}	1.31×10^{-4}
900	8×10^{-14}	1.6×10^{-9}	5×10^{-5}	1.04×10^{-4}
1000	1.0×10^{-13}	3.5×10^{-9}	2.9×10^{-5}	8.8×10^{-5}
1100	1.5×10^{-13}	5.5×10^{-9}	2.7×10^{-5}	8.0×10^{-5}
1200	2.0×10^{-13}	6.5×10^{-9}	3.1×10^{-5}	7.4×10^{-5}
1300	-	8.5×10^{-9}	-	7.1×10^{-5}

Our prior work on reaction 2 was investigated up to 1000 K.[11] Higher temperatures were not studied due to concerns of thermal dissociation. However, after measuring the $O^- + N_2$ rate constant up to 1200 K, we extended the measurements of reaction 2 up to higher temperatures. Representative data appears in Figure 4. No clear evidence of thermal decomposition was found. At 1200 K this is in accordance with the literature indicating that the half-life of N_2O at is ~30 ms, about five times the length of the experiment.[25] At 1300 K, the literature half-life is just 1.5 ms, which should result in a measurable decrease in N_2O concentration and a commensurate decrease in attachment. However, this is not

apparent in the results, which reasonably follow Arrhenius equation behavior. Still, the highest temperature results here should be interpreted cautiously. The determined rate constants increasingly deviated from our prior reported values[11] as temperature was increased, despite being measured using the same apparatus and nominally the same procedure. The present results were consistent over attempts spanning several weeks. We were unable to conclusively reconcile the discrepancy but consider the present values to supersede those previously reported. Both the previously reported and present values appear in Table 1 and Figure 5.

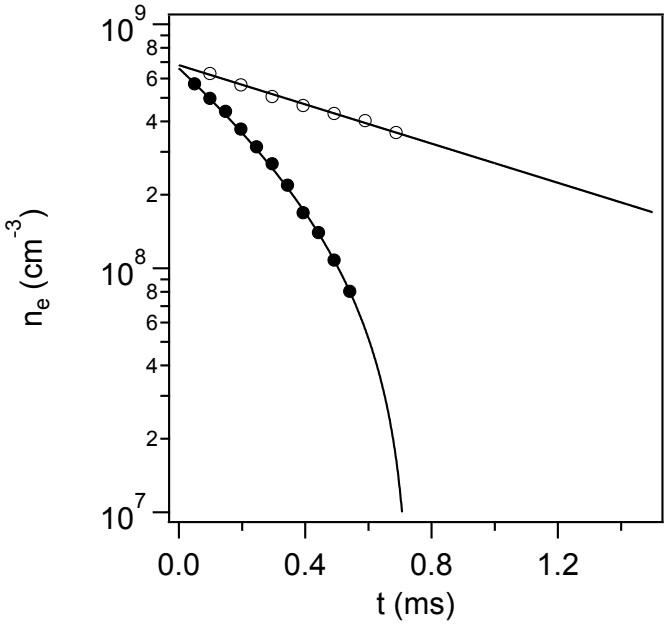

Figure 4. Representative data of electron density as a function of reaction time at 1200 K and 1.7 Torr. Open points are without N_2O present indicating a diffusion rate constant of 925 s^{-1}. Solid points are with 2.3 $\times 10^{11}$ cm^{-3} of N_2O present and indicate an electron attachment rate constant of 7 $\times 10^{-9}$ cm^3 s^{-1}. Curves are best fits to the data.

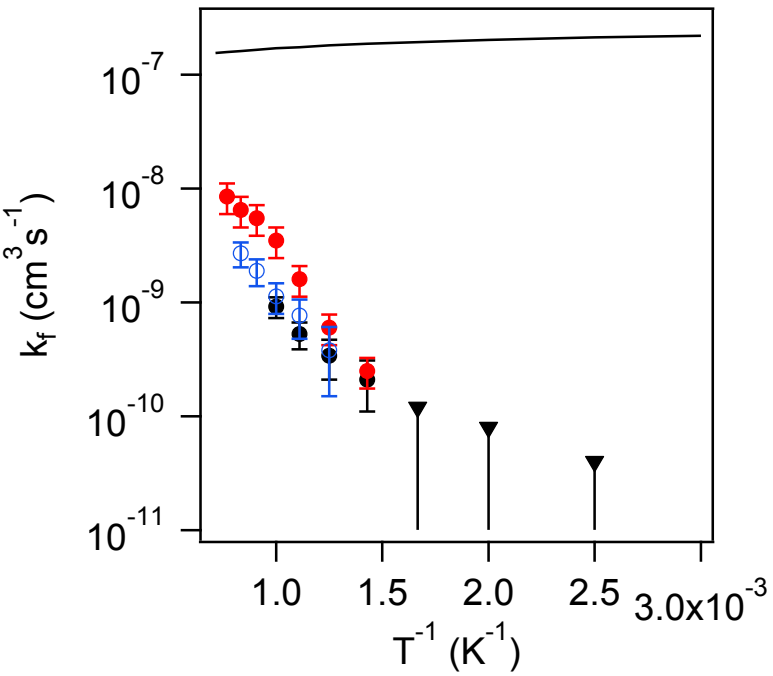

Figure 5. Measured k_{N2O+e-} as a function of inverse temperature from the present data (solid red circles) and previously published data (solid black circles; black triangles indicate upper limits) along with values derived from equilibrium with k_{O-+N2} (blue open circles). Curve is the calculated collision rate.

Reactions 1 and 2 are reverse reactions of one another and can be related by microscopic reversibility. The equilibrium constants for the reaction as a function of temperature were calculated and details presented in the SI. Care must be taken in calculating the thermicity of the reaction from enthalpies of formation that values employing either the "electron convention" or the "ion convention" in the treatment of the electron enthalpy are not mixed. Additionally, the electron here is treated using Fermi-Dirac statistics as detailed by Bartmess.[26] Reaction 1 is exothermic by about 22 kJ mol^{-1} at room temperature, but this value decreases with increasing temperature and the reaction becomes endothermic above about 1450 K. Reaction 1 has a decrease in entropy of about 106 J mol^{-1} K^{-1} at room temperature, with the change becoming smaller as temperature increases. Reaction 1 is endergonic at room temperature by about 9 kJ mol^{-1} and becomes increasingly disfavored as temperature increases such that the equilibrium favors $O^- + N_2$. Interestingly, the calculated equilibrium constant reaches a minimum at about 1500 K and then increases, although investigation of N_2O at such high a temperature would be prohibitive as the half-life to thermal decomposition is ~10 μs. Results are shown in Table S2 and Figures S1 - S4.

Inherent to both associative detachment and electron attachment processes is a crossing between the neutral and anion surfaces. Here, we calculate the potential energy surfaces of N_2O and N_2O^- at the CCSD(T) level to further understand the reaction dynamics occurring. A semi-quantitative picture of the N_2O and N_2O^- potential surfaces was deduced decades ago.[27] Full surfaces were calculated using early *ab initio* methods and a minimum energy crossing point (MECP) identified at r_{NN} = 1.18 Å, r_{NO} = 1.28 Å, and Θ = 154°, values all quite close to the average of the N_2O and N_2O^- equilibrium structures, at an

energy of 0.4 ±0.1 eV above the N_2O minimum. These results are in good agreement with present calculations at the CCSD(T) level, especially considering the tools available in 1978. At a given Θ, the surfaces form a crossing seam as shown in Figures 6 and 7. The seam "translates" from high energy structures with small r_{NN} and r_{NO} bond lengths at smaller Θ, through a lower energy region, and then back to a high energy region at large r_{NN} and r_{NO} bond lengths at larger Θ. The full crossing between these states of the neutral and anion is a three-dimensional surface, reaching a minimum at Θ = 151° shown in Figure 7. The electronic energy of the MECP lies 0.62 eV above that of the N_2O minimum using the aug-cc-pVTZ basis set and is lowered to 0.57 eV by CBS extrapolation for aug-cc-pVXZ (X=3,4,5). It is not obvious how to account for zero-point energy in this comparison. We note that the MECP lies very close to being along the normal mode for a bending vibration of N_2O and it is reasonable to expect that the best comparison is excluding the zero-point energy of this one mode, lowering the MECP to 0.53 eV above the minimum.

The energies of the N_2O and N_2O^- minima are very similar, with the adiabatic electron affinity of N_2O being close to zero, although the specific value has a long history of debate. The most recent experimental determinations[28–31] date back to the 1970's and 1980's and suggest a small, likely positive electron affinity. More recent theoretical[32] work indicates a small negative electron affinity, with the Active Thermochemical Tables[33] adopting an adiabatic value of -9.1 ±2.9 kJ mol^{-1} to form a weakly bound $O^-(N_2)$ structure and -13.2 ±1.9 kJ mol^{-1} to the metastable N_2O^- structure of more interest here. Calculations here at the CCSD(T)/CBS (aug-cc-pVXZ X=3,4,5) // CCSD(T)/aug-cc-pVTZ level yield values of -3.6 kJ mol^{-1} and -14.3 kJ mol^{-1}, respectively (Figure S6).

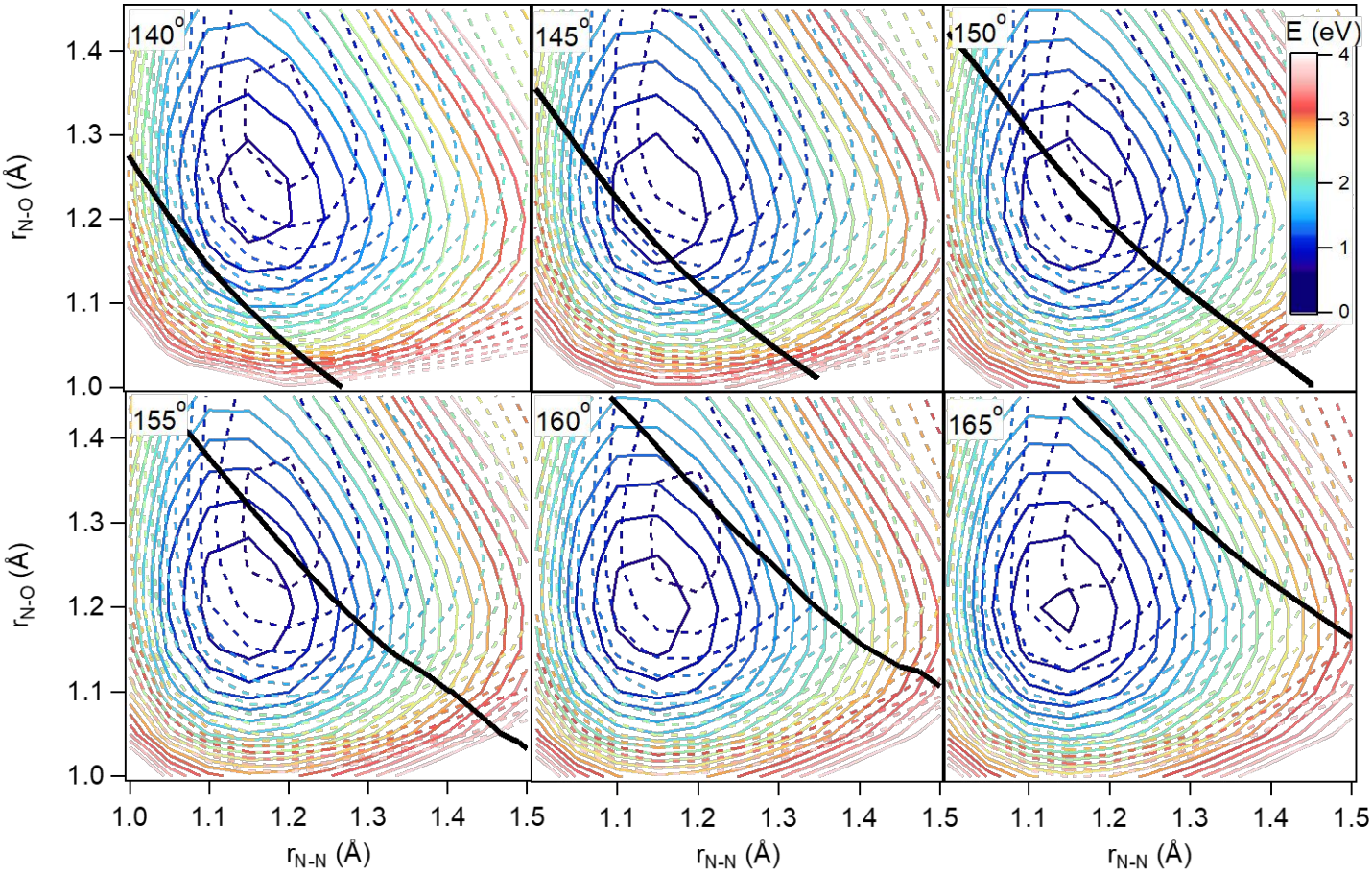

Figure 6. Regions of the potential energy surfaces of N_2O (solid lines) and N_2O^- (dashed lines) with Θ = 140° – 165° calculated at the CCSD(T)/aug-cc-pVTZ level. Energies are relative to the N_2O minimum. Solid black curves indicate crossing seams. Contours are spaced by 0.2 eV.

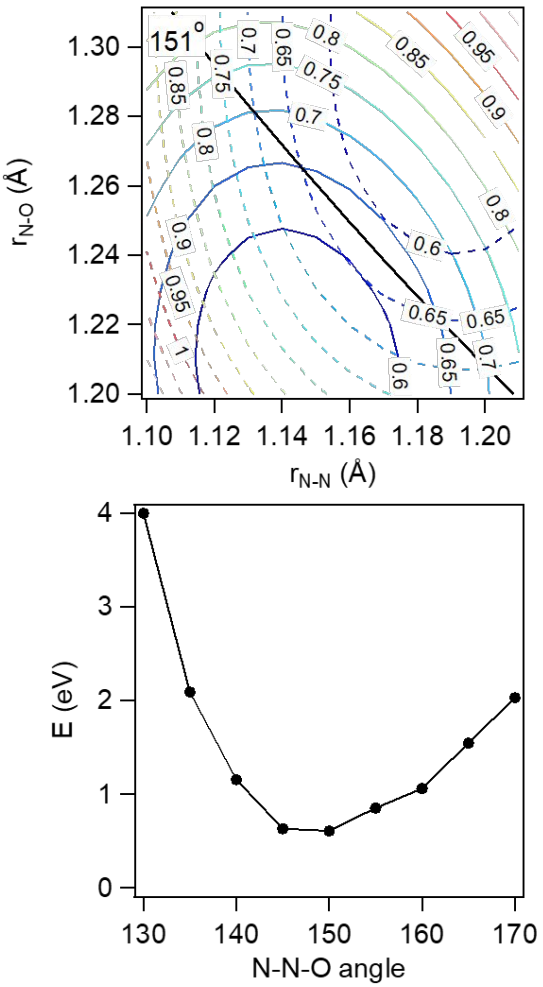

Figure 7. Top) Region of the potential energy surfaces of N_2O (solid lines) and N_2O^- (dashed lines) with $\Theta = 151^o$ in the region of the minimum energy crossing point calculated at the CCSD(T)/aug-cc-pVTZ level. Contours are spaced by 0.05 eV. The solid black curve indicates the crossing seam. Bottom) Energy of the minimum crossing point between the N_2O and N_2O^- surfaces as a function of the N-N-O angle Θ.

As noted elsewhere,[32,34] there is a substantial barrier between N_2O^- and the $O^-(N_2)$ exit complex. The minimum energy profile of N_2O^- as a function of the r_{N-O} distance is shown in Figure 8. The energy of the transition state is nearly identical to the energy of the MECP between the N_2O and N_2O^- surfaces, with a CBS ZPE-corrected value of 0.52 eV For most of the potential surfaces, the T1 diagnostic[35] is small, but rises to a moderate value of 0.04 at the N_2O^- barrier and of 0.03 at the MECP indicating some multireference character.

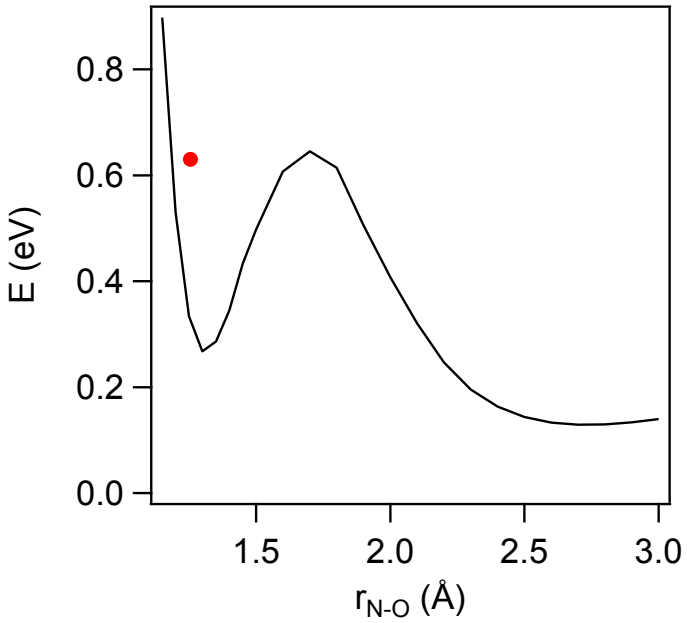

Figure 8. Minimum electronic energy profile of the N_2O^- system as a function of the r_{N-O} coordinate calculated at the CCSD(T)/aug-cc-pvtz level showing the N_2O^- well near 1.3 Å and the $O^-(N_2)$ well near 2.7 Å. The location of the MECP with the N_2O ground state surface is indicated (red circle, not on the minimum energy path). Energies are relative to the electronic energy of the N_2O minimum; zero-point corrections are not included.

Discussion

The rate constant of reaction 1 is found to increase steeply with temperature but remains highly inefficient over the range measured. The largest reported rate constant of 2×10^{-13} cm^3 s^{-1} at 1200 K corresponds to ~1 reactive event out of every 5,000 collisions. Comparing the rate constants derived above with the previous drift tube experiments[6] requires understanding of the various energy distributions. The present experiment involves pure temperature so all forms of energy are described by Boltzmann distributions. In a drift tube, various effective temperatures apply and one has to worry about how distributions differ from thermal. These have been explained in detail previously.[36,37] Briefly, an effective center of mass kinetic energy is given by the Wannier expression

$$\frac{3}{2}kT_{eff} = \frac{3}{2}kT_0 + \frac{1m_i + m_b}{2m_i + m_n}m_n v_d^2 \quad (3)$$

where T_{eff} is an effective translational temperature, k is the Boltzmann constant, m_i is the mass of the reactant ion, m_n is the mass of the reactant neutral, m_b is the mass of the buffer species, and v_d is the drift velocity. The drift velocity is a function on the applied electric field (E/n) and the reduced ion mobility (κ_0)

$$v_D = \kappa_0(E/n)N_0 \quad (4)$$

where N_0 is the Loschmidt constant, the ideal gas number density at standard conditions. In He buffers the distribution at T_{eff} is close to what is found at an equivalent temperature but the distribution in heavier buffers is distinct from thermal ones. For instance, for the reaction of O^+ with N_2, which has a similar

steep rate of increase in the rate constant as a function of temperature, the rate constants in an Ar buffer are up to 3 times higher than those in a helium buffer for the same T_{eff}.[38] The present data is compared to the drift tube measurements of R&M as a function of T_{eff} in Figure 9; the agreement is poor.

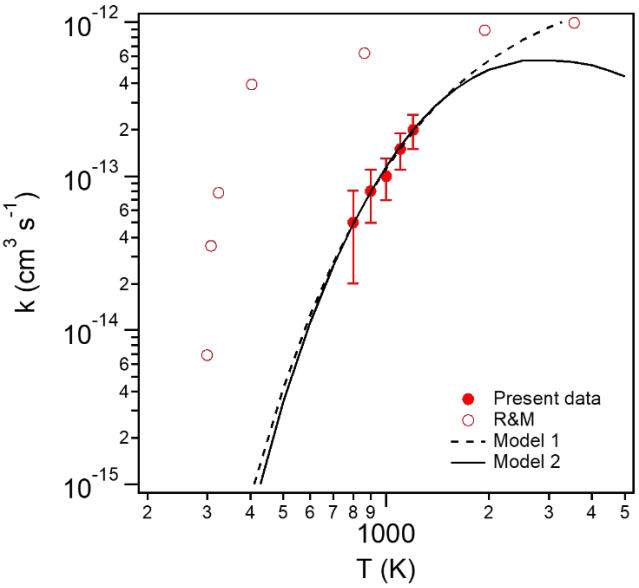

Figure 9. Comparison of rate constants of reaction 1, $O^- + N_2 \rightarrow N_2O + e^-$, from the present data (solid circles) as a function of temperature and the drift tube values reported by R&M (open circles) ref. [6] as a function of effective translational temperature (see text). Fits to the present data (curves) are as described in the text.

The pathway for reactions 1 and 2 requires surmounting two energetic barriers: the transition state between $O^-(N_2)$ and N_2O^- and the crossing from the anion to the neutral surface, both about 0.5 eV above the N_2O minimum. Assuming Arrhenius equation behavior for $N_2O + e^-$, the present data yields an activation energy of 0.48 eV, very close to the calculated barriers. Two prior studies, including our own, report smaller activation energies of 0.2 – 0.3 eV; these are inconsistent with the potential surfaces presented here.[11,12] Assuming Arrhenius equation behavior for reaction 1, the present data yields an activation energy of 0.28 eV, very close to both the vibrational frequency of N_2 (0.29 eV) and the calculated energetic barrier relative to the $O^- + N_2$ asymptote (0.31 eV).

J&P deduced that the reactivity observed by R&M was primarily due to reaction with vibrationally excited N_2. If we assume that all reactivity observed here is due to N_2 (v=1) (i.e. that v = 0 is unreactive and that v > 1 populations are negligible, the rate constant at a given temperature is $k_{v1}*P(T,v_1)$. This yields a very good fit to the data (Figure 9, model 1) and implies a temperature-independent rate constant for $O^- + N_2(v=1)$ of $k = 3\times10^{-12}$ cm^3 s^{-1}. A somewhat more complex model may be constructed by inspection of the N_2O^- potential energy surface (Figure 10).

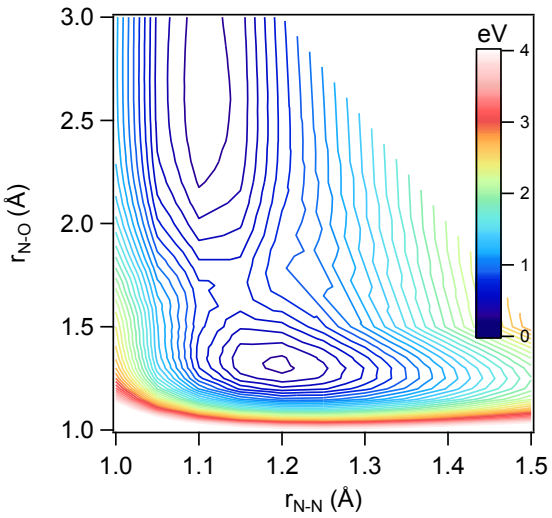

Figure 10. Slice of the N_2O^- potential surface at $\Theta = 135^o$ calculated at the CCSD(T)/aug-cc-pVTZ level. Energies are relative to the N_2O neutral minimum. Contour spacing is 0.1 eV.

The slice of the potential surface presented in Figure 10 offers an interesting variation on the Polanyi reaction rules.[39] The $O^- + N_2$ reaction has an "early" barrier, such that translational energy would generally promote reaction to a greater extent than would vibrational energy. However, the saddle point is offset from the entrance valley centered at the N_2 equilibrium bond length of $r_{NN} = 1.09$ Å. The N_2 must be elongated as it approaches the O^- in order to access the transition state, and this is more likely under vibrational excitation. The transition state between $O^-(N_2)$ and N_2O^- lies at ~$r_{NN} = 1.14$ Å and $r_{NO} = 1.60$ Å over a broad range of angles Θ (Figure S7 and S8). Integrating the product of the probability density functions of a harmonic oscillator with the N_2 vibrational frequency and an Arrhenius equation with an activation energy equal to the most favorable energy on the reactant-product ridge at the r_{NN} on the N_2O^- potential surface (Figure 11) yields vibrational state specific rate constants (see SI for more description). The probability of crossing to the neutral surface is accounted for in the manner detailed by Troe for electron attachment processes, a function decaying exponentially with the collision velocity (see SI) including an adjustable parameter to fit to the data.[40] Summing these weighted by the vibrational populations reproduces the experimental rate constants well (Figure 9, model 2). The vibrationally-resolved rate constants derived in this manner appear in Figure 12 and Table S3. The v=0 rate constant is very small at room temperature, rising steeply so that about half of the observed reactivity at that temperature is due to v=0 even though the rate constant is still small, ~10^{-13} cm^3 s^{-1}. The v=1 rate constant has much less temperature-dependence because in this model the activation energy is effectively smaller for the excited state. The rate constant across the measured range of temperatures is ~2×10^{-12} cm^3 s^{-1}, in agreement with that derived by the simpler method above. The values for v=2 have large uncertainty as not much of that state is populated and relies only the above analysis. The negative temperature dependence of the v = 2 rate constant is due to the decreasing crossing probability at higher temperatures and is also apparent in the modeled total rate constant (Figure 9, model 2) at extreme temperatures. Assuming these vibrationally-resolved rate constants, the fraction of vibrationally excited N_2 in the R&M experiment can be estimated (Figure S9) and rises linearly with the applied drift field. Further evaluation of the vibrational effect could be achieved through state-selected experiments or through theory via trajectory or direct dynamics calculations. The rate constant extrapolated to room temperature is ~10^{-17} cm^3 s^{-1}, with large uncertainty, and may be directly measurable using an ion trap.

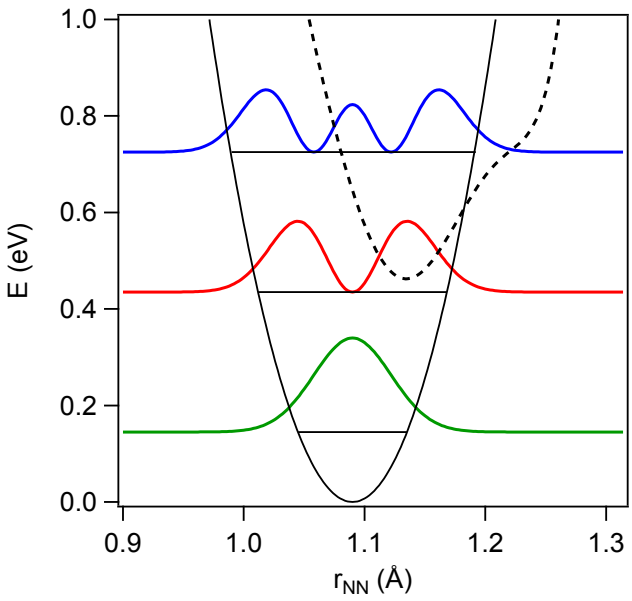

Figure 11. Harmonic potential of N_2 (solid line) and probability density functions for v=0 (green), 1 (red), and 2 (blue) overlayed with the shape of the potential surface near the saddle point (dashed line) at $\Theta = 135^{o}$.

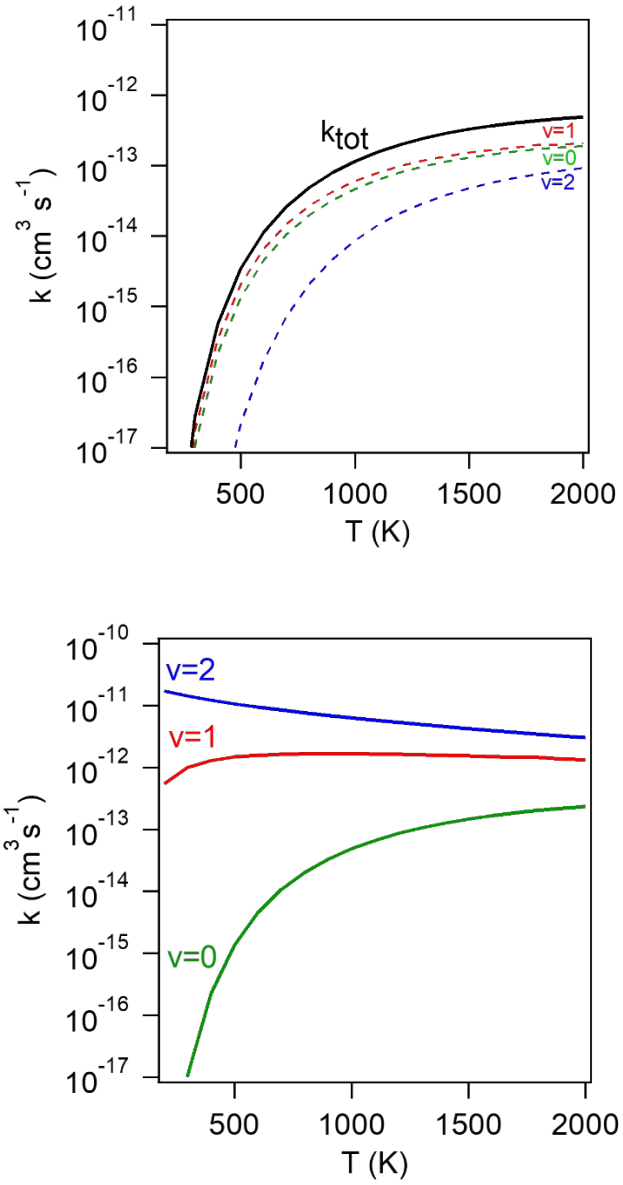

Figure 12. Derived rate constants for reaction 1, $O^- + N_2$ from 'model 2' as described in the text. Top) Total rate constant (black solid curve) and contribution from v = 0 (green dashed), v = 1 (red dashed), v = 2 (blue dashed). Bottom) Vibrational state specific rate constants for reaction 1 for v = 0 (green), v = 1 (red), and v = 2 (blue).

In the same spirit as above, the attachment kinetics for reaction (2) are well-modeled using a simple framework. The MECP lies quite close to the N_2O bending vibration normal mode. Treating the activation energy as the energy of the MECP less the energy in an N_2O bending mode and summing across the vibrational populations of the two bending modes υ_2^0 and υ_2^1

$$k(T) = k_{coll}(T)\sum_{m.n} P_{m,n}(T)\left(e^{\frac{-E_a(m)}{kT}} + e^{\frac{-E_a(n)}{kT}} - e^{\frac{-E_a(m)-E_a(n)}{kT}}\right) \quad (5)$$

$$E_a(x) = E_{MECP} - xE(\upsilon_2) \quad (6)$$

where $k_{coll}(T)$ is the calculated collision rate constant of $e^- + N_2O$ using an analytical form of the extended Vogt-Wannier framework,[41,42] $P_{m,n}(T)$ is the thermal population of the bending mode vibrational states υ_2^0=m and υ_2^1=n, and E_{mecp} is the energy of the MECP relative to the N_2O minimum (0.53 eV). Summing equation (5) through the first seven levels of each bending mode results in the fit shown in Figure 13. We note that the fit is largely indistinguishable from a simple Arrhenius equation fit. The agreement with the present experimental values is very good, supporting that excitation of the bending modes enhances reactivity.[43] Literature results at lower temperatures[14] are in excellent agreement with the model, while those at higher temperatures[13] are consistent, although with large apparent uncertainty. Not shown is the data of Mullen et al.[15] at still higher temperatures, which are in modest agreement, but carry very large uncertainty.

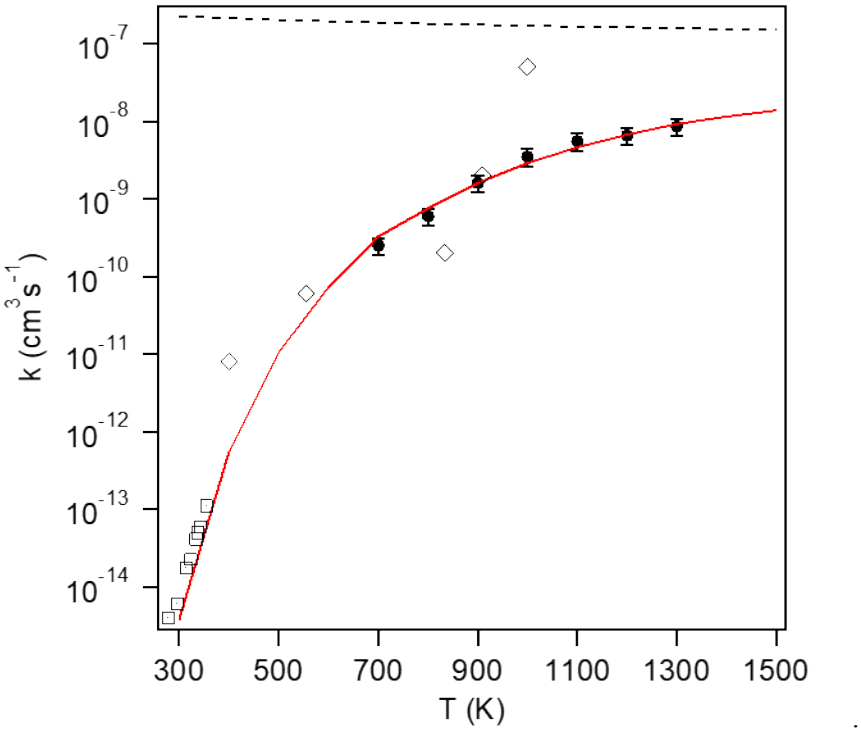

Figure 13. Rate constants for reaction (2) $N_2O + e^-$ as a function of temperature from the present experiment (solid circles), the model described in the text (red curve), and literature values from Warman et al.[14] (open squares) and Chantry[13] (open diamonds). Dashed curve is the calculated collisional rate constant.

Experimentally derived and calculated equilibrium constants between reactions (1) and (2) are shown in Table 1. They do not agree, with the calculated values being 2 – 3 times larger (the older attachment rate constants published by our group[11] provide better agreement, but we believe this was fortuitous). A reasonable interpretation is that one, or more likely both, reactions have significantly non-thermal product distributions. This is of course not a statement that microscopic reversibility fails, but that the microscopic processes linking the thermally populated states $O^- + N_2$ and $N_2O + e^-$ do not

dominate the overall rate constants of the reactions. As a result, accurate rate constants of reaction (1) are not accessible from the measurements of reaction (2) coupled with the calculated equilibrium constants.

The small rate constant for reaction (1) suggests that associative detachment with N_2 will not dominate the destruction of O^- in upper atmospheric TLE. Ternary association of O^- with O_2 to form O_3^- [44] should remain the dominant process above pressures of ~100 mTorr (up to ~65 km). At altitudes above ~80 km, the dissociative attachment process

$$O^- + O \rightarrow O_2 + e^- \quad (7)$$

which proceeds at a substantial fraction of the Langevin rate is most significant.[45,46] At altitudes in-between, several processes could be contributing, including

$$O^- + CO \rightarrow CO_2 + e^- \quad (8)[47]$$

$$O^- + H_2 \rightarrow H_2O + e^- \quad (9)[47]$$

$$O^- + O_2(^1\Delta_g) \rightarrow O_3 + e^- \quad (10a)[48,49]$$

$$O^- + O_2(^1\Delta_g) \rightarrow O_2 + O_2^- \quad (10b)$$

$$O^- + CO_2 + M \rightarrow CO_3^- + M \quad (11)[44].$$

More details on implications for TLE will be published in the geophysics literature.

Conclusions

The kinetics of the associative detachment reaction $O^- + N_2$ and the reverse dissociative attachment reaction $N_2O + e^-$ have been measured up to 1300 K using a flowing afterglow apparatus. The $O^- + N_2$ rate constants are very small, rise steeply with temperature, and are in disagreement with the previous literature values. It is likely that N_2 vibrational excitation enhances the reaction rate and that a prior analysis of the literature values concluding that the results were affected by vibrationally excited N_2 is correct.[5] Vibrationally-resolved rate constants are derived from the present results.

The $N_2O + e^-$ rate constants also rise steeply with temperature, described by an activation energy of 0.5 eV. The reaction must overcome two energetic barriers, a crossing to the anion surface and a barrier to dissociation, both of which are calculated to be ~0.5 eV. The experimental rate constants are well-described by assuming that reactivity is enhanced by excitation of the N_2O bending modes.

These results impact modeling of transient luminous events in the mesosphere. Likely, the $O^- + N_2$ associative detachment process does not appreciably occur as previously assumed. Alternative reactions with CO, H_2, CO_2, $O_2(^1\Delta_g)$, or O should be considered depending on the altitude of interest.

Author Contributions

NSS: Formal analysis, Funding acquisition, Investigation, Methodology, Writing – original draft; TMM: Investigation, Methodology, Writing – review & editing; SGA: Writing – review & editing; AAV: Funding acquisition, Conceptualization, Methodology, Writing – review & editing.

Conflicts of interest

There are no conflicts to declare.

Acknowledgments

This work is supported by the Air Force Office of Scientific Research for support under AFOSR-22RVCOR009. TMM is supported through the Institute for Scientific Research of Boston College under contract No. FA9453-20-C-0048. We thank Reza Janalizadeh for bringing the questions concerning the associative detachment to our attention.
The views expressed are those of the authors and do not reflect the official guidance or position of the Department of the Air Force, the Department of Defense (DoD), or the United States government. The appearance of external hyperlinks does not constitute endorsement by the United States DoD of the linked websites, or the information, products, or services contained therein. The DoD does not exercise any editorial, security, or other control over the information you may find at these locations.

References

(1) Gordillo-Vazquez, F. J.; Perez-Invernon, F. J. A Review of the Impact of Transient Luminous Events on the Atmospheric Chemistry: Past, Present, and Future. *Atmos. Res.* **2021**, *252*, 105432.

(2) Luque, A.; Gordillo-Vazquez, F. J. Mesospheric Electric Breakdown and Delayed Sprite Ignition Caused by Electron Detachment. *Nat. Geosci.* **2012**, *5*, 22–25.

(3) Winkler, H.; Notholt, J. A Model Study of the Plasma Chemistry of Stratospheric Blue Jets. *J. Atmos. Solar-Terrestrial Phys.* **2015**, *122*, 75–85.

(4) Liu, N. Multiple Ion Species Fluid Modeling of Sprite Halos and the Roleof Electron Detachment of O^- in Their Dynamics. *J. Geophys. Res.* **2012**, *117*, A03308.

(5) Janalizadeh, R.; Pasko, V. P. Implications of Electron Detachment in Associative Collisions of Atomic Oxygen Anion with Molecular Nitrogen for Modeling of Transient Luminous Events. *Geophys. Res. Lett.* **2020**, *48*, e2020GL091134.

(6) Rayment, S. W.; Moruzzi, J. L. Electron Detachment Studies between O- and Nitrogen. *Int. J. Mass Spectrom. Ion Process.* **1978**, *26*, 321–326.

(7) Fehsenfeld, F. C.; Ferguson, E. E.; Schmeltekopf, A. L. Thermal-Energy Associative-Detachment Reactions of Negative Ions. *J. Chem. Phys.* **1966**, *45*, 1844.

(8) Lindinger, W.; Albritton, D. L.; Fehsenfeld, F. C.; Ferguson, E. E. Reactions of O^- with N_2, N_2O, SO_2, NH_3, CH_4, and C_2H_4 and $C_2H_2^-$ with O_2 from 300 °K to Relative Kinetic Energies of ∼2 EV. *J. Chem. Phys.* **1975**, *63*, 3238–3242.

(9) Comer, J.; Schulz, G. J. Measurements of Electron-Detachment Cross Sections from O^- and S^-.

Phys. Rev. A **1975**, *10*, 2100–2106.

(10) Doussot, C.; Bastien, F.; Marode, E.; Moruzzi, J. L. A New Technique for Studying Ion Conversion and Detachment Reactions in Oxygen and in O_2/SO_2 and O_2/N_2Bmixtures. *J. Phys. D-Applied Phys.* **1982**, *16*, 2451–2461.

(11) Sawyer, J. C.; Miller, T. M.; Ard, S. G.; Sweeny, B. C.; Viggiano, A. A.; Shuman, N. S. Thermal Rate Constants for Electron Attachment to N2O: An Example of Endothermic Attachment. *J. Chem. Phys.* **2020**, *153*, 074306.

(12) Brüning, F.; Matejcik, S.; Illenberger, E.; Chu, Y.; Senn, G.; Muigg, D.; Denifl, G.; Märk, T. D. Effects of Temperature on the Dissociative Electron Attachment to N_2O. *Chem. Phys. Lett.* **1998**, *292*, 177–182.

(13) Chantry, P. J. Temperature Dependence of Dissociative Attachment in N2O. *J. Chem. Phys.* **1969**, *51* (8), 3369–3379.

(14) Warman, J. M.; Fessenden, R. W.; Bakale, G. Dissociative Attachment of Thermal Electrons to N_2O and Subsequent Electron Detachment. *J. Chem. Phys.* **1972**, *57*, 2702–2711.

(15) Mullen, J. H.; Madson, J. M.; Medgyesi-Mitschand, L. N. Measurement of Electron Attachment Processes in a High-Temperature Plasma. *Proc. IEEE* **1971**, *59*, 605–607.

(16) Moruzzi, J. L.; Ekin, J. W.; Phelps, A. V. Electron Production by Associative Detachment of O^- Ions with NO, CO, and H_2. *J. Chem. Phys.* **1968**, *48*, 3070.

(17) Miller, T. M.; Friedman, J. F.; Williamson, J. S.; Schaffer, L. C.; Viggiano, A. A. A New Instrument for Thermal Electron Attachment at High Temperature: NF_3 and CH_3Cl Attachment Rate Constants up to 1100 K. *Rev. Sci. Instrum.* **2009**, *80*, 34104.

(18) Hosl, A.; Pachin, J.; Eguz, E.; Chachereau, A.; Franck, C. M. Measurement and Modeling of Electron and Anion Kinetics in N2O Discharges. *J. Phys. D-Applied Phys.* **2020**, *53*, 135202.

(19) McFarland, M.; Dunkin, D. B.; Fehsenfeld, F. C.; Schmeltekopf, A. L.; Ferguson, E. E. Collisional Detachment Studies of NO−. *J. Chem. Phys.* **1972**, *56*, 2358.

(20) Bierbaum, V. M.; Grabowski, J. J.; DePuy, C. H. Gas-Phase Synthesis and Reactions of Nitrogen- and Sulfur-Containing Anions. *J. Phys. Chem.* **1984**, *88*, 1389–1393.

(21) Troe, J.; Miller, T. M.; Viggiano, A. A. Low-Energy Electron Attachment to SF(6). II. Temperature and Pressure Dependences of Dissociative Attachment. *J. Chem. Phys.* **2007**, *127*, 244304.

(22) Ham, H.-C.; Ariyageadsakul, P.; Baeck, K. K. Thermochemistry of Neutral and Anionic Sulfur Fluorides SF_n (n = 1–6): Revisited with Theoretical G4/W1/W2 Composite Methods and the Roles of Metastable Conformer of SF_4^- Anion. *AIP Adv.* **2020**, *10*, 125112.

(23) Chen, C. L.; Chantry, P. J. Temperature Dependence of SF_6^-, SF_5^-, and F^- Production from SF_6/. *Bull. Am. Phys. Soc.* **1970**, *15*, 418.

(24) Frisch, M. J.; Trucks, G. W.; Schlegel, H. B.; Scuseria, G. E.; Robb, M. A.; Cheeseman, J. R.; Scalmani, G.; Barone, V.; Petersson, G. A.; Nakatsuji, H.; Li, X.; Caricato, M.; Marenich, A. V; Bloino, J.; Janesko, B. G.; Gomperts, R.; Mennucci, B.; Hratchian, H. P.; Ortiz, J. V; Izmaylov, A. F.; Sonnenberg, J. L.; Williams-Young, D.; Ding, F.; Lipparini, F.; Egidi, F.; Goings, J.; Peng, B.; Petrone, A.; Henderson, T.; Ranasinghe, D.; Zakrzewski, V. G.; Gao, J.; Rega, N.; Zheng, G.; Liang, W.; Hada, M.; Ehara, M.; Toyota, K.; Fukuda, R.; Hasegawa, J.; Ishida, M.; Nakajima, T.;

Honda, Y.; Kitao, O.; Nakai, H.; Vreven, T.; Throssell, K.; Montgomery Jr., J. A.; Peralta, J. E.; Ogliaro, F.; Bearpark, M. J.; Heyd, J. J.; Brothers, E. N.; Kudin, K. N.; Staroverov, V. N.; Keith, T. A.; Kobayashi, R.; Normand, J.; Raghavachari, K.; Rendell, A. P.; Burant, J. C.; Iyengar, S. S.; Tomasi, J.; Cossi, M.; Millam, J. M.; Klene, M.; Adamo, C.; Cammi, R.; Ochterski, J. W.; Martin, R. L.; Morokuma, K.; Farkas, O.; Foresman, J. B.; Fox, D. J. Gaussian 16 . C.01. Gaussian Inc.: Wallingford, CT 2016.

(25) Gerhard, L.; Wargadalam, V. J.; Winter, F.; Hofbauer, H. Decomposition of Nitrous Oxide at Medium Temperatures. *Combust. Flame* **2000**, *120*, 427–438.

(26) Bartmess, J. E. Thermodynamics of the Electron and the Proton. *J. Phys. Chem.* **1994**, *98*, 6420–6424.

(27) Bardsley, J. N. Negative Ions of N_2O and CO_2. *J. Chem. Phys.* **1969**, *51*, 3384–3389.

(28) Nalley, S. J.; Compton, R. N.; Schweinler, H. C.; Anderson, V. E. Molecular Electron Affinities from Collisional Ionization of Cesium. I. NO, NO_2, and N_2O. *J. Chem. Phys.* **1973**, *59*, 4125.

(29) Coe, J. V.; Snodgrass, J. T.; Freidhoff, C. B.; McHugh, K. M.; Bowen, K. H. Negative Ion Photoelectron Spectroscopy of N_2O^- and $(N_2O_2)^-$. *Chem. Phys. Lett.* **1986**, *124*, 274–278.

(30) Wentworth, W. E.; Chen, E.; Freeman, R. Thermal Electron Attachment to N_2O. *J. Chem. Phys.* **1971**, *55*, 2075.

(31) Tiernan, T. O.; Wu, R. L. C. Thermochemical Data for Molecular Negative Ions from Collisional Dissociation Thresholds. *Adv. Mass Spectrom.* **1978**, *7A*, 136.

(32) Kryachko, E. S.; Vinckier, C.; Nguyen, M. T. Another Look at the Electron Attachment to Nitrous Oxide. *J. Chem. Phys.* **2001**, *114*, 7911–7917.

(33) Ruscic, B.; Bross, D. H. *Active Thermochemical Tables (ATcT) based on ver. 1.124 of the Thermochemical Network (2023); available at ATcT.anl.gov*. https://atct.anl.gov.

(34) Suter, H. U.; Greber, T. On the Dissociation of N_2O after Electron Attachment. *J. Phys. Chem. B* **2004**, *108*, 14511–14517.

(35) Lee, T. J.; Taylor, P. R. A Diagnostic for Determining the Quality of Single-Reference Electron Correlation Methods. *Int. J. Quantum Chem.* **1989**, *36*, 199–207.

(36) Viehland, L. A.; Viggiano, A. A.; Mason, E. A. The Ar^+-He Interaction Potential And Distribution Function Effects on Swarm Measurements of $Ar^+ + N_2$ Reaction-Rate Coefficients Using Helium Buffer Gas. *J. Chem. Phys.* **1991**, *95*, 7286–7297.

(37) Albritton, D. L. Energy Dependences of Ion-Neutral Reactions Studied in Drift Tubes. In *Kinetics of Ion-Molecule Reactions*; 1979; pp 119–142.

(38) Rowe, B. R.; Fahey, D. W.; Fehsenfeld, F. C.; Albritton, D. L. Rate Constants for the Reactions of Metastable O^{+*} Ions with N_2 and O_2 at Collision Energies 0.04 to 0.2 EV and the Mobilities of These Ions at 300 K. *J. Chem. Phys.* **1980**, *73*, 194–205.

(39) Polanyi, J. C. Some Concepts in Reaction Dynamics. *Acc. Chem. Res.* **1972**, *5*, 161–168.

(40) Troe, J.; Marowsky, G.; Shuman, N. S.; Miller, T. M.; Viggiano, A. A. On the Temperature Dependence of the Thermal Electron Attachment to SF6, SF5Cl, and POCl3. *Z. Phys. Chem.* **2011**, *225*, 1405–1416.

(41) Dashevskaya, E. I.; Litvin, I.; Nikitin, E. E.; Troe, J. Electron Capture by Polarizable Dipolar

Targets: Numerical and Analytically Approximated Capture Probabilities. *J. Phys. Chem. A* **2011**, *115*, 6825–6830.

(42) Dashevskaya, E. I.; Litvin, I.; Nikitin, E. E.; Troe, J. Modelling Low-Energy Electron-Molecule Capture Processes. *Phys. Chem. Chem. Phys.* **2008**, *10*, 1270–1276.

(43) Allan, M.; Skalicky, T. Structures in Elastic, Vibrational, and Dissociative Electron Attachment Cross Sections in N_2O near Threshold. *J. Phys. B At. Mol. Opt. Phys.* **2003**, *36*, 3397–3409.

(44) Ikezoe, Y.; Matsuoka, D.; Takebe, M.; Viggiano, A. A. *Gas Phase Ion-Molecule Reaction Rate Constants Through 1986*; Maruzen: Tokyo, 1987.

(45) Ard, S. G.; Melko, J. J.; Jiang, B.; Li, Y. L.; Shuman, N. S.; Guo, H.; Viggiano, A. A. Temperature Dependences for the Reactions of O_2^- and O^- with N and O Atoms in a Selected-Ion Flow Tube Instrument. *J. Chem. Phys.* **2013**, *139*, 144302.

(46) Fehsenfeld, F. C.; Schmeltekopf, A. L.; Schiff, H. I.; Ferguson, E. E. Laboratory Measurements of Negative Ion Reactions of Atmospheric Interest. *Planet. Space Sci.* **1967**, *15*, 373–379.

(47) McFarland, M.; Albritton, D. L.; Fehsenfeld, F. C.; Ferguson, E. E.; Schmeltekopf, A. L. Flow-Drift Technique for Ion Mobility and Ion-Molecule Reaction-Rate Constant Measurements 3. Negative-Ion Reactions of O^- with CO, NO, H_2, and D_2. *J. Chem. Phys.* **1973**, *59*, 6629–6635.

(48) Fehsenfeld, F. C.; Albritton, D. L.; Burt, J.; Schiff, H. I. Associative-Detachment Reactions of O^- and O_2^- by $O_2(^1\Delta_G)$. *Can. J. Chem.* **1968**, *47*, 1793–1795.

(49) Midey, A.; Dotan, I.; Viggiano, A. A. Temperature Dependences for the Reactions of O^- and O_2^- with $O_2(a^1\Delta_g)$ from 200 to 700 K. *J. Phys. Chem. A* **2008**, *112*, 3040–3045.